Research Article Vol. 14, No. 4 / 1 Apr 2024 / Optical Materials Express 871
Optical Materials EXPRESS

On the applicability of the Maxwell Garnett effective medium model to media with a high density of cylindrical pores

JULIA BRANDT,[1,*] GUIDO DITTRICH,[2,3] MARC THELEN,[2,3] HAGEN RENNER,[1] PATRICK HUBER,[2,3] MANFRED EICH,[1,4] AND ALEXANDER PETROV[1,4]

[1]Hamburg University of Technology, Institute of Optical and Electronic Materials, Eißendorfer Straße 38, 21073 Hamburg, Germany
[2]Hamburg University of Technology, Institute for Materials and X-Ray Physics, Denickestraße 10, 21073 Hamburg, Germany
[3]Center for X-Ray and Nano Science CXNS, Deutsches Elektronen-Synchrotron DESY, Notkestraße 85, 20355 Hamburg, Germany
[4]Institute of Functional Materials for Sustainability, Helmholtz-Zentrum Hereon, 21502 Geesthacht, Germany
*julia.brandt@tuhh.de

Abstract: The optical properties of dielectric materials with subwavelength cylindrical pores are commonly described by effective medium models. We compare the Maxwell Garnett and the Bruggeman effective medium models for porous silicon with simulations and experiments for the case of polarization orthogonal to the pore axis. The Maxwell Garnett model matches the results of the simulations even up to very high porosities. An experimental study of the effective permittivity of macroporous and mesoporous silicon is conducted by analyzing the Fabry-Pérot oscillations in the long-wavelength limit. These experimental results are also consistent with the Maxwell Garnett model. We advocate using this model for media with cylindrical pores in the future.

1. Introduction

Homogenizing physical properties of a composite or a structured medium has been a subject of scientific research for many decades. For the electromagnetic and optical properties of media composed of structures which are much smaller than the wavelength, the most commonly used effective medium models are the Maxwell Garnett model [1] and the Bruggeman model [2]. Both these models are based on the polarizability of spherical or cylindrical inclusions and simple assumptions about average electric fields. Other homogenization techniques involve more complex averaging methods of electromagnetic fields or energy and can be applied analytically [3,4] or numerically [5,6]. When the structure size increases and becomes comparable to the incident wavelength, more intricate methods are required, like the energy coherent potential approximation [7,8] or T-Matrix based approaches [9,10]. Similarly, effective medium models fail to describe structures which exhibit surface plasmon resonances or those containing strong evanescent fields [11]. The latter can even occur in purely dielectric structures [12–14].

Optical effective medium models have been an important tool to characterize a transparent structured or a porous medium to validate its fabrication method. Typically, experimentalists measure the phase velocity of light propagating in such a medium [15]. In this case, a valid effective medium model is essential to conclude a particular parameter, e.g. the porosity from interference Fourier transform spectroscopy during imbibition processes [16] or the liquid filling fraction from capillary condensation [17]. One group of such media are those with densely packed

#516125 https://doi.org/10.1364/OME.516125
Journal © 2024 Received 15 Dec 2023; revised 24 Jan 2024; accepted 24 Jan 2024; published 5 Mar 2024

Optical Materials EXPRESS

cylindrical pores, usually arranged in a hexagonal lattice, as sketched in Fig. 1(a). Examples of such media are porous silicon, porous anodized aluminum oxide and porous germanium [18–20]. With their adjustable porosity, these media can be the basis for creating functional materials with tunable optical properties [21–24]. For example, a liquid confined in membranes with cylindrical pores can show extraordinary properties which are absent in the unconfined liquid [25]. Generally, the pores are parametrized by the pore diameter d, the interpore distance a and the porosity p. Due to the parallel pore alignment, such a porous medium is optically anisotropic with the optic axis along the pores. The ordinary refractive index is equal to the one for the orthogonal direction of polarization relative to the cylindrical axis, while the extraordinary refractive index corresponds to the polarization parallel to the cylindrical axis.

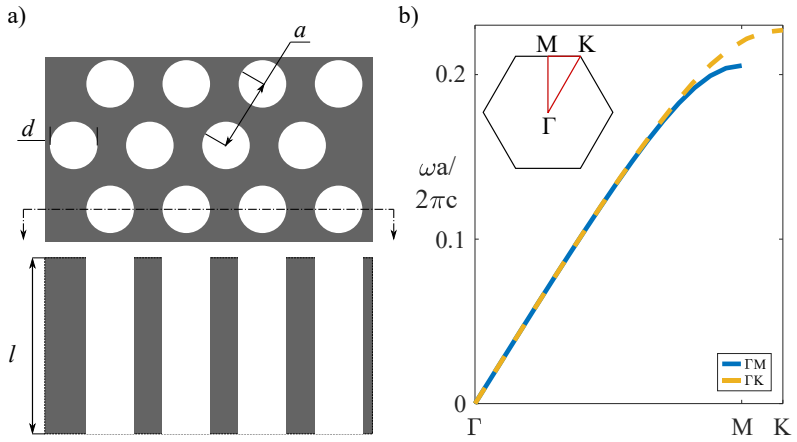

Fig. 1. a) Schematic of the top and side view of a membrane of thickness l, with a periodic arrangement of cylindrical pores of diameter d, and lattice constant a; b) First photonic band of a hexagonal lattice of air pores in silicon with porosity 0.5 along the ΓM and ΓK directions with the electric field orthogonal to the cylindrical axis; inset shows the Brillouin zone of this structure with the directions of the k-vector indicated.

Here, we consider the application of the Maxwell Garnett effective medium model in the long-wavelength regime to structures with a high density of cylindrical pores. Our focus is on air pores in silicon; however, it can be applied to other material combinations as well. We consider the polarization orthogonal to the cylinders, which is typically assessed by excitation normal to the surface. As the model considers a single cylinder to be in a constant electric field, it is generally expected that the Maxwell Garnett model fails if the cylinders are close to each other. Consequently, the Bruggeman model is the usual method of choice to analyze structures of high porosity [26–28]. However, it is known from numerical and analytical approximations that the Maxwell Garnett model is robust also for high filling fractions up to the point of touching spherical [29,30] or cylindrical inclusions [31,32].

In this paper, we analyze different effective medium models for media with cylindrical pores for the case of orthogonal polarization and compare them to simulations with an eigenmode solver. We demonstrate the superiority of the Maxwell Garnett effective medium model over the Bruggeman model, even for high porosity. Additionally, we show experimentally determined the effective permittivity for orthogonal polarization from porous silicon membranes which correspond well to these numerical results.

Optical Materials EXPRESS

2. Effective medium models and simulation

One way to derive an effective medium model of a composite is to identify the electric and displacement field average over its volume. When the volume under consideration is much smaller than the wavelength of the incident light, then a quasistatic approximation can be used where the volume is placed in a constant external electric field. In some cases, the average internal fields in each of the constituents can be obtained analytically. The internal electric field is related to an external electric field by a geometry-dependent factor A, which we refer to as the field enhancement factor. From the volume-averaged displacement field divided by the volume-averaged electric field, the effective permittivity can be retrieved using Eq. (1):

$$\varepsilon_{\text{eff}} = \frac{A_{\text{air}}\, p\, \varepsilon_{\text{air}} + A_{\text{Si}}(1-p)\varepsilon_{\text{Si}}}{A_{\text{air}}\, p + A_{\text{Si}}(1-p)} \tag{1}$$

shown exemplarily for an air-silicon composite with p being the filling fraction of air and ε_{air} and ε_{Si} being the permittivity of air and silicon, respectively.

For cylindrical particles in a medium two electric field polarizations must be distinguished: the polarization orthogonal and the polarization parallel to the cylindrical axis. In case the electric field is polarized parallel to the cylindrical axis, the field enhancement factors are $A = A_{\text{air}} = A_{\text{Si}} = 1$ such that the internal electric field is equal to the external field. As this is true regardless of further assumptions, the parallel effective permittivity is equal in both Maxwell Garnett and Bruggeman models. Equation (2) denotes the permittivity for this polarization direction:

$$\varepsilon_{\text{eff},\parallel} = p\, \varepsilon_{\text{air}} + (1-p)\varepsilon_{\text{Si}} \tag{2}$$

For the polarization perpendicular to the cylinder axis, the two models give different effective permittivities. In the scope of the Maxwell Garnett model, a composite consists of inclusions inside a host medium. The particles are fully surrounded by the host medium and do not interact with each other. For the case that the electric field is polarized orthogonal to the cylindrical axis, the field enhancement factors are $A_{\text{air}} = 2\varepsilon_{\text{Si}}/(\varepsilon_{\text{air}} + \varepsilon_{\text{Si}})$ and $A_{\text{Si}} = 1$ [33]. Equation (3) shows the effective permittivity for this case:

$$\varepsilon_{\text{eff},\perp} = \varepsilon_{\text{Si}} \frac{(1-p)\varepsilon_{\text{Si}} + (1+p)\varepsilon_{\text{air}}}{(1+p)\varepsilon_{\text{Si}} + (1-p)\varepsilon_{\text{air}}} \tag{3}$$

In contrast, Bruggeman's effective medium model presumes shape equality between the individual components of the composite. Each component, in our case air and silicon, is assumed to be surrounded by the effective medium itself. This approach is expected to account for the interactions between the inclusions. The model considers all components to have the same shape and, thus, cylindrical field enhancement factors of $A_{\text{air}} = 2\varepsilon_{\text{eff},\perp}/(\varepsilon_{\text{air}} + \varepsilon_{\text{eff},\perp})$ for the air pores, and $A_{\text{Si}} = 2\varepsilon_{\text{eff},\perp}/(\varepsilon_{\text{Si}} + \varepsilon_{\text{eff},\perp})$ for silicon. As a consequence, this model is fully symmetric with respect to an interchange of permittivity and porosity. The geometrical assumption of cylindrical shape, however, is clearly not fulfilled for the silicon part of the structure.

Equation (4a) is the Bruggeman equation of the orthogonal permittivity, presented in a form analogous to that of Eq. (3). It facilitates the identification of the field enhancement factors. In the literature, the Bruggeman equation is often given in the form of Eq. (4b), which is equivalent to Eq. (4a). Both equations are implicit. To simplify the calculation, we give an explicit expression for the orthogonal effective permittivity in Eq. (4c).

$$\varepsilon_{\text{eff},\perp} = \frac{p\varepsilon_{\text{air}}(\varepsilon_{\text{Si}} + \varepsilon_{\text{eff},\perp}) + (1-p)\varepsilon_{\text{Si}}(\varepsilon_{\text{air}} + \varepsilon_{\text{eff},\perp})}{p(\varepsilon_{\text{Si}} + \varepsilon_{\text{eff},\perp}) + (1-p)(\varepsilon_{\text{air}} + \varepsilon_{\text{eff},\perp})} \tag{4a}$$

$$\frac{\varepsilon_{\text{Si}} - \varepsilon_{\text{eff},\perp}}{\varepsilon_{\text{Si}} + \varepsilon_{\text{eff},\perp}}(1-p) + \frac{\varepsilon_{\text{air}} - \varepsilon_{\text{eff},\perp}}{\varepsilon_{\text{air}} + \varepsilon_{\text{eff},\perp}}\, p = 0 \tag{4b}$$

Optical Materials EXPRESS

$$\varepsilon_{\mathrm{eff},\perp} = \frac{1}{2}\left[(1-2p)(\varepsilon_{\mathrm{Si}}-\varepsilon_{\mathrm{air}}) + \sqrt{(1-2p)^2(\varepsilon_{\mathrm{Si}}-\varepsilon_{\mathrm{air}})^2 + 4\varepsilon_{\mathrm{Si}}\varepsilon_{\mathrm{air}}}\right] \tag{4c}$$

In porous media, the cylindrical pores can form a hexagonal lattice with lattice constant a (Fig. 1(a)). Electromagnetic modes in a periodic medium can be described as Bloch modes, with a dispersion relation defined as a set of frequencies ω which can propagate through the lattice with a particular wavevector k. Such a dispersion relation or band structure of a photonic crystal can be calculated numerically. We used the eigenmode solver "MIT Photonic Bands (MPB)" [34]. In Fig. 1(b) we show the first photonic band of the hexagonal arrangement of air pores in silicon along the directions of high symmetry ΓM and ΓK. The electric field is polarized orthogonal to the cylindrical axis and the respective permittivity values are $\varepsilon_{\mathrm{Si}} = 12.25$ and $\varepsilon_{\mathrm{air}} = 1$. The inset of Fig. 1(b) shows the Brillouin-zone of the lattice and these points of high symmetry. At k-values small as compared to $2\pi/a$, ω is directly proportional to k and the curves coincide as straight lines in all directions. The ratio of ω to k has the meaning of the phase velocity in the medium, from which we obtain the effective refractive index of the porous membrane. Since silicon is non-magnetic, it holds for the effective permittivity that $\varepsilon_{\mathrm{eff}} = n_{\mathrm{eff}}^2$.

We have calculated the effective permittivity of porous silicon for the case where the incident polarization is orthogonal to the cylindrical axis. The permittivity along the ΓM and ΓK directions are equal apart from numerical noise. The porosity is derived from the geometry of a single pore with pore diameter d in the hexagonal unit cell. If $d = a$ or larger, the cylinders would touch or overlap and the membrane would lose connectivity, thus, collapse. The highest physically obtainable porosity for these membranes is $p_{\max} = \pi/2\sqrt{3}$.

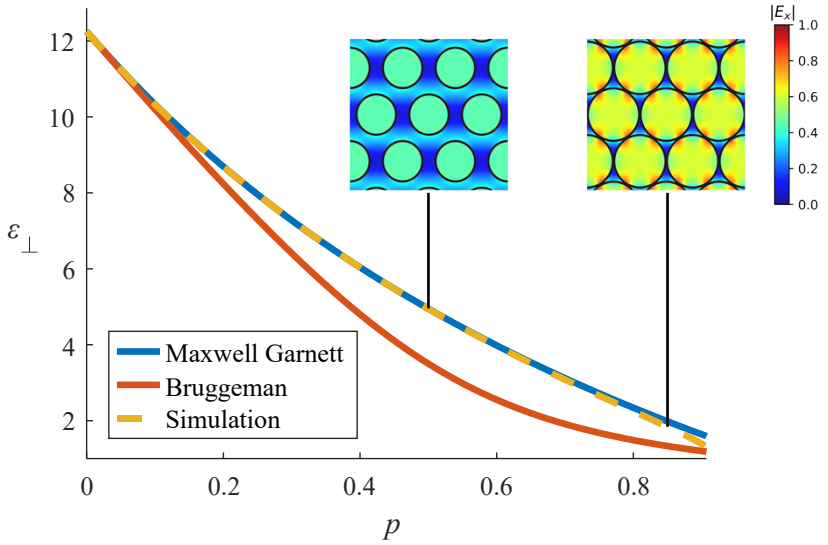

Fig. 2. The effective permittivity for orthogonal polarization calculated from the Maxwell Garnett and the Bruggeman model, as well as from simulations. The insets show the simulated absolute value of the x-component of the electric field inside the structure

Figure 2 shows the effective permittivity of porous silicon in air for the polarization orthogonal to the cylindrical axis as a function of porosity. The effective permittivity is calculated using both the Maxwell Garnett (solid blue line) and Bruggeman (solid red line) models, as well as numerical simulations (dashed yellow line). Remarkably, we see an almost perfect match between the result from the Maxwell Garnett model and the one from the simulations, even up to high porosity values. For porosities higher than 0.3, the Bruggeman model returns a significantly

Optical Materials EXPRESS

lower effective permittivity. This deviation can be explained by the wrong assumption on the field enhancement in silicon and the overestimation of the influence the pores have on one another.

Additionally, in the inset of Fig. 2 we show the absolute value of the x-component of the electric field at two different porosities: for $p = 0.5$ and for $p = 0.85$. At $p = 0.5$, the electric field is constant within each pore and is not influenced by the neighboring pores. At $p = 0.85$, on the other hand, the behavior is notably different: overall, the pores are much closer to each other, we can see strong field enhancements in the areas where the pores are close, and the magnitude of the average electric field is only slightly larger than in the case of small pores. Thus, the deviation from the Maxwell Garnett model is only moderate.

3. Experiments

To confirm the applicability of the Maxwell Garnett model to media with a high density of cylindrical pores, we experimentally study two sample systems of porous silicon: macroporous and mesoporous silicon. The macroporous silicon membrane (purchased from SmartMembranes GmbH) is fabricated by photoelectrochemical etching of a prepatterned n-type silicon wafer; this method is described elsewhere [35]. The pore diameter, interpore distance and membrane thickness are verified by scanning electron microscopy to be $d = 1.1$ µm, $a = 1.5$ µm and $\mathrm{l} = 46$ µm, correspondingly. The image of the top surface (Fig. 3(a)) shows a square-shaped pore entrance, which results from the prepatterning with the mask, but this shape transitions into a cylindrical pore within approximately 1 µm, as can be seen from the side view (Fig. 3(d)). The pores at the bottom surface are widened due to the lift-off procedure [36] (Fig. 3(b)). This widening is, however, limited to a few micrometers while the pore remains cylindrical (Fig. 3(e)). Despite this structural difference to the assumptions made within the effective medium models, we believe that the experimentally measured permittivity should still match the theoretical one calculated with the with the average porosity. This porosity is determined gravimetrically to be $p = 0.41$.

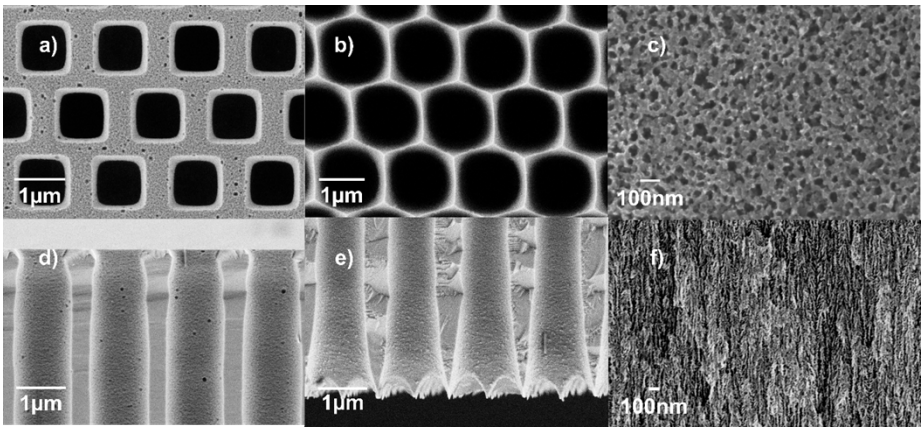

Fig. 3. Macroporous silicon (a) top view; b) bottom view; d) side view from top area, e) side view from bottom area) and mesoporous silicon (c) top view; f) side view) imaged with a scanning electron microscope.

Two mesoporous silicon membranes are fabricated by electrochemical anodization of single crystalline (100), p-doped silicon wafers (boron doped, 10-20 mΩcm, purchased from Si-Mat) in a volumetric 2:3 mixture of 48% hydrofluoric acid (HF) solution and ethanol. During the self-organized growth of the nanometer sized pores, a depletion of charge carriers, known as the quantum wire effect [37], limits a further dissolution of the pore wall material. However, there is a finite increase in porosity for longer etching times. For samples thicker than 10 µm, the

Optical Materials EXPRESS

etching time scales linearly with the sample thickness. Two samples were prepared. Sample 1 was synthesized by applying a constant current density of 12.5 mA/cm^2 for 25.5 min. To obtain a free-standing porous membrane from the wafer, the current density was increased to 400 mA/cm^2 and applied for 20 s. Sample 2 was fabricated with a pulsed etching technique: the fabrication started with 0 mA/cm^2 for 6 min followed by pulsed etching with alternating current densities of 0 mA/cm^2 and 12.5 mA/cm^2 applied for 1 s each. In total, a current density of 12.5 mA/cm^2 was applied for 53 min. For the detachment, the etching solution was exchanged for a 9:29 mixture of HF (48%): ethanol. A constant current density of 6 mA/cm^2 was applied for 240 s.

We chose a different synthesis procedure for sample 2 to reduce pore widening which occurs at a longer etching time. It should be noted that in mesoporous silicon membranes, the pores are, in fact, not periodically aligned (Fig. 3(c)) nor are perfectly cylindrical (Fig. 3(f)). Rather, the pores only have a short-range order which can be characterized by an average interpore distance. Additionally, the pores are slightly conical [38] and show dendritic branching [39].

We retrieve the effective permittivity of these porous silicon membranes from spectrometric measurements with light being incident normal to the surface. The membrane can be considered a Fabry-Pérot resonator with a free spectral range $\Delta\nu$. From the condition of constructive interference, the effective refractive index can be approximated as the group refractive index and from this, the effective permittivity is calculated:

$$\varepsilon_{\mathrm{eff},\perp} = n^2_{\mathrm{eff},\perp} \approx \left(\frac{c}{2l\Delta\nu}\right)^2 \tag{5}$$

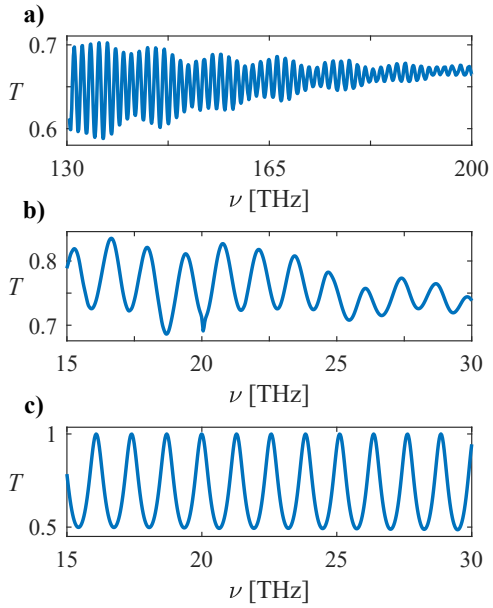

Fig. 4. Experimental transmission spectra of a) the mesoporous silicon sample 1 of porosity 0.55 and 53 µm thickness, and b) the macroporous silicon membrane of porosity 0.41 and 46 µm thickness; c) Simulated transmission spectrum of the macroporous silicon membrane.

The specular transmission spectrum of the macroporous silicon membrane was recorded with an FTIR spectrometer (Vertex70, Bruker Optics) in the wavelength range $\lambda = 10 - 20\,\mu$m; the transmission spectra of the mesoporous silicon samples were obtained using a UV-Vis-NIR spectrometer (Lambda 1050, Perkin Elmer) in the wavelength range $\lambda = 1.4 - 2.2\,\mu$m. We have chosen frequency ranges where the dispersion of silicon is weak and the material loss is

Optical Materials EXPRESS

as small as $1.8\,\mathrm{cm}^{-1}$ in the MIR [41] and $3.5{\cdot}10^{-8}\,\mathrm{cm}^{-1}$ in the NIR [42] frequency range, and therefore, negligible over the membrane thickness. Additionally, we simulated the transmission spectrum of the macroporous silicon membrane with the frequency domain solver from the CST Studio Suite package [40]. For this, we implemented the structure and the parameters of the macroporous silicon sample ($d = 1.1$ µm, $a = 1.5$ µm and $l = 46$ µm) and we set the permittivity to $\varepsilon_{\mathrm{Si,MIR}} = 11.70$ for silicon for the MIR frequency range. Figure 4(a) shows the experimentally recorded transmission spectra of the mesoporous silicon sample. For the macroporous silicon sample 1, we plot the transmission spectrum in Fig. 4(b) and the corresponding simulated transmission spectrum in Fig. 4(c). All curves show well-defined Fabry-Pérot oscillations. The maxima in the experimental results do not reach unity due to losses from diffuse scattering.

The experimental effective permittivity was calculated from an average $\Delta\nu$ between the maxima of the oscillation using Eq. (5). We considered a permittivity of $\varepsilon_{\mathrm{Si,IR}} = 12.08$ and of $\varepsilon_{\mathrm{Si,MIR}} = 11.70$ for the effective medium calculation for the respective NIR [42] and MIR [41] frequency ranges. The experimental and effective medium results are listed in Table 1. The experimental results match well with the values from the Maxwell Garnett model, while deviating more than 20% from the Bruggeman model. Although the mesoporous membrane shows a rather three-dimensional porous network instead of straight cylindrical pores, there is still a cylindrical preferential direction with circular holes in the polar plane which leads to the good agreement with the Maxwell Garnett model. The effective permittivity obtained from the simulation of the porous silicon membrane is 5.62, which is close to the Maxwell Garnett model, as well.

Table 1. Effective permittivity for the polarization orthogonal to the pore

Sample	Experimental result	Maxwell Garnett Model	Bruggeman Model
Macroporous Si			
0.41 porosity	5.86	5.66	4.49
46 µm thickness			
Mesoporous Si 1			
0.55 porosity	4.33	4.37	2.96
53 µm thickness			
Mesoporous Si 2			
0.47 porosity	5.19	5.15	3.80
22 µm thickness			

4. Conclusion

Our work has demonstrated that the effective permittivity of media with cylindrical pores retrieved from simulations for the case of orthogonal polarization match the Maxwell Garnett model with remarkably high accuracy. By contrast, and likely because of an overestimation of the influence the pores have on each other, the results of the Bruggeman model largely deviate from those of the simulations. Experimental results with macroporous and mesoporous silicon also agree very well with the Maxwell Garnett model. Based on this outcome, we argue for the application of the Maxwell Garnett model over the Bruggeman model for media with cylindrical pores at low and high porosity. With this work, we hope to resolve a long-standing misconception in the application of the Maxwell Garnett and the Bruggeman models to these systems and provide a simple solution.

Funding. Deutsche Forschungsgemeinschaft (192346071); Technische Universität Hamburg (Funding Programme Open Access Publishing).

Acknowledgement. The authors thank Dassault Systèmes for providing their simulation software "CST Studio Suite". We thank Iris Bucher for acquiring the SEM images of the macroporous silicon sample.

Optical Materials EXPRESS

Disclosures. The authors have no conflicts to disclose.

Data Availability. Data underlying the results presented in this paper are not publicly available at this time but may be obtained from the authors upon reasonable request.

References

1. J. C. Maxwell Garnett, "XII. Colours in metal glasses and in metallic films," Phil. Trans. R. Soc. Lond. A **203**(359-371), 385–420 (1904).
2. D. A. G. Bruggeman, "Berechnung verschiedener physikalischer Konstanten von heterogenen Substanzen. I. Dielektrizitätskonstanten und Leitfähigkeiten der Mischkörper aus isotropen Substanzen," Ann. Phys. **416**(7), 636–664 (1935).
3. L. D. Landau and E. M. Lifshitz, "Electrostatics of dielectrics," in *Electrodynamics of Continuous Media* (Elsevier, 1984), pp. 34–85.
4. H. Looyenga, "Dielectric constants of heterogeneous mixtures," Physica **31**(3), 401–406 (1965).
5. R. C. McPhedran and D. R. McKenzie, "The conductivity of lattices of spheres I. The simple cubic lattice," Proc. R. Soc. Lond. A **359**(1696), 45–63 (1978).
6. B. W. Ninham and R. A. Sammut, "Refractive index of arrays of spheres and cylinders," J. Theor. Biol. **56**(1), 125–149 (1976).
7. K. Busch and C. M. Soukoulis, "Transport properties of random media: a new effective medium theory," Phys. Rev. Lett. **75**(19), 3442–3445 (1995).
8. K. Busch and C. M. Soukoulis, "Transport properties of random media: an energy-density CPA approach," Phys. Rev. B **54**(2), 893–899 (1996).
9. B. Zerulla, R. Venkitakrishnan, and D. Beutel, "A T-matrix based approach to homogenize artificial materials," Adv. Opt. Mater. **11**(3), 2201564 (2023).
10. V. Popov, A. V. Lavrinenko, and A. Novitsky, "Operator approach to effective medium theory to overcome a breakdown of Maxwell Garnett approximation," Phys. Rev. B **94**, 085428 (2016).
11. P. A. Belov, R. Marqués, S. I. Maslovski, *et al.*, "Strong spatial dispersion in wire media in the very large wavelength limit," Phys. Rev. B **67**(11), 113103 (2003).
12. H. Herzig Sheinfux, I. Kaminer, Y. Plotnik, *et al.*, "Subwavelength multilayer dielectrics: ultrasensitive transmission and breakdown of effective-medium theory," Phys. Rev. Lett. **113**(24), 243901 (2014).
13. T. Dong, J. Luo, H. Chu, *et al.*, "Breakdown of Maxwell Garnett theory due to evanescent fields at deep-subwavelength scale," Photon. Res. **9**(5), 848 (2021).
14. R. Mei, J. Qin, D. Yan, *et al.*, "Breakdown of effective-medium theory in dielectric composites containing epsilon-near-zero constituents," Phys. Rev. B **109**(4), 045104 (2024).
15. M. J. Sailor, *Porous Silicon in Practice* (Wiley, 2011).
16. L. G. Cencha, R. Urteaga, and C. L. A. Berli, "Interferometric technique to determine the dynamics of polymeric fluids under strong confinement," Macromolecules **51**(21), 8721–8728 (2018).
17. A. V. Kityk, K. Knorr, and P. Huber, "Liquid n-hexane condensed in silica nanochannels: A combined optical birefringence and vapor sorption isotherm study," Phys. Rev. B **80**(3), 035421 (2009).
18. L. Canham, *Handbook of Porous Silicon* (Springer International Publishing, 2018).
19. K. Nielsch, J. Choi, K. Schwirn, *et al.*, "Self-ordering regimes of porous alumina: the 10 porosity rule," Nano Lett. **2**(7), 677–680 (2002).
20. A. Dupuy, M. R. Aziziyan, D. Machon, *et al.*, "Anisotropic mesoporous germanium nanostructures by fast bipolar electrochemical etching," Electrochim. Acta **378**, 137935 (2021).
21. C. Pacholski, "Photonic crystal sensors based on porous silicon," Sensors **13**(4), 4694–4713 (2013).
22. V. S. Lin, K. Motesharei, K. P. Dancil, *et al.*, "A porous silicon-based optical interferometric biosensor," Sensors **278**(5339), 840–843 (1997).
23. D. Schmidt and M. Schubert, "Anisotropic Bruggeman effective medium approaches for slanted columnar thin films," J. Appl. Phys. **114**(8), 8 (2013).
24. L. G. Cencha, G. Dittrich, P. Huber, *et al.*, "Precursor film spreading during liquid imbibition in nanoporous photonic crystals," Phys. Rev. Lett. **125**(23), 234502 (2020).
25. P. Huber, "Soft matter in hard confinement: phase transition thermodynamics, structure, texture, diffusion and flow in nanoporous media," J. Phys.: Condens. Matter **27**, 103102 (2015).
26. A. M. Campos, J. Torres, and J. J. Giraldo, "Porous silicon dielectric function modeling from effective medium theories," Surf. Rev. Lett. **09**(05n06), 1631–1635 (2002).
27. M. Khardani, M. Bouaïcha, and B. Bessaïs, "Bruggeman effective medium approach for modelling optical properties of porous silicon: comparison with experiment," Phys. Status Solidi (c) **4**(6), 1986–1990 (2007).
28. V. Torres-Costa and R. J. Martín-Palma, "Application of nanostructured porous silicon in the field of optics. a review," J Mater Sci **45**(11), 2823–2838 (2010).
29. C. M. Soukoulis, S. Datta, and E. N. Economou, "Propagation of classical waves in random media," Phys. Rev. B **49**(6), 3800–3810 (1994).
30. N. J. Hutchinson, T. Coquil, A. Navid, *et al.*, "Effective optical properties of highly ordered mesoporous thin films," Thin Solid Films **518**(8), 2141–2146 (2010).

Optical Materials EXPRESS

31. A. Kirchner, K. Busch, and C. M. Soukoulis, "Transport properties of random arrays of dielectric cylinders," Phys. Rev. B **57**(1), 277–288 (1998).
32. H. Karimian-Sarakhs and M. H. Neshati, "Comparative analysis of the effective permittivity of aligned cylindrical perforated substrate," in *2020 28th Iranian Conference on Electrical Engineering (ICEE)* (IEEE, 2020), pp. 1–4.
33. A. H. Sihvola, *Electromagnetic Mixing Formulas and Applications* (Institution of Electrical Engineers, 2008).
34. S. Johnson and J. Joannopoulos, "Block-iterative frequency-domain methods for Maxwell's equations in a planewave basis," Opt. Express **8**(3), 173–190 (2001).
35. V. Lehmann and H. Föll, "Formation mechanism and properties of electrochemically etched trenches in n-Type silicon," J. Electrochem. Soc. (Journal of The Electrochemical Society) **137**(2), 653–659 (1990).
36. W. Lang, P. Steiner, and H. Sandmaier, "Porous silicon: a novel material for microsystems," Sensors and Actuators A: Physical **51**(1), 31–36 (1995).
37. V. Lehmann and U. Gösele, "Porous silicon formation: a quantum wire effect," Appl. Phys. Lett. **58**(8), 856–858 (1991).
38. M. Thelen, N. Bochud, M. Brinker, *et al.*, "Laser-excited elastic guided waves reveal the complex mechanics of nanoporous silicon," Nat. Commun. **12**(1), 3597 (2021).
39. M. Brinker, M. Thelen, M. May, *et al.*, "How nanoporous silicon-polypyrrole hybrids flex their muscles in aqueous electrolytes: In operando high-resolution X-ray diffraction and electron tomography-based micromechanical computer simulations," Phys. Rev. Materials **6**(11), 116002 (2022).
40. Dassault Systèmes, CST Studio Suite (2023).
41. D. Chandler-Horowitz and P. M. Amirtharaj, "High-accuracy, midinfrared (450cm−1⩽ω⩽4000cm−1) refractive index values of silicon," J. Appl. Phys. **97**(12), 12 (2005).
42. M. A. Green and M. J. Keevers, "Optical properties of intrinsic silicon at 300 K," Prog. Photovolt: Res. Appl. **3**(3), 189–192 (1995).